Radiofrequency Ablation for Treating Chronic Pain of Bones: Effects of Nerve Locations

Singh, S. and Melnik, R.

In: Rojas I., Valenzuela O., Rojas F., Ortuño F. (eds), Bioinformatics and Biomedical Engineering: Lecture Notes in Computer Science book series (LNCS, volume 11466), IWBBIO, pp. 418-429, Springer, 2019.

Radiofrequency Ablation for Treating Chronic Pain of Bones: Effects of Nerve Locations

Sundeep Singh[1] and Roderick Melnik[1,2(✉)]

[1] MS2Discovery Interdisciplinary Research Institute, Wilfrid Laurier University, 75 University Avenue West, Waterloo, ON N2L 3C5, Canada
rmelnik@wlu.ca

[2] BCAM - Basque Center for Applied Mathematics, Alameda de Mazarredo 14, 48009 Bilbao, Spain

Abstract. The present study aims at evaluating the effects of target nerve location from the bone tissue during continuous radiofrequency ablation (RFA) for chronic pain relief. A generalized three-dimensional heterogeneous computational model comprising of muscle, bone and target nerve has been considered. The continuous RFA has been performed through the monopolar needle electrode placed parallel to the target nerve. Finite-element-based coupled thermo-electric analysis has been conducted to predict the electric field and temperature distributions as well as the lesion volume attained during continuous RFA application. The quasi-static approximation of the Maxwell's equations has been used to compute the electric field distribution and the Pennes bioheat equation has been used to model the heat transfer phenomenon during RFA of the target nerve. The electrical and thermo-physical properties considered in the present numerical study have been acquired from the well-characterized values available in the literature. The protocol of the RFA procedure has been adopted from the United States Food and Drug Administration (FDA) approved commercial devices available in the market and reported in the previous clinical studies. Temperature-dependent electrical conductivity along with the piecewise model of blood perfusion have been considered to correlate with the *in-vivo* scenarios. The numerical simulation results, presented in this work, reveal a strong dependence of lesion volume on the target nerve location from the considered bone. It is expected that the findings of this study would assist in providing *a priori* critical information to the clinical practitioners for enhancing the success rate of continuous RFA technique in addressing the chronic pain problems of bones.

Keywords: Bone · Chronic pain · Continuous radiofrequency ablation · Nerve ablation · Computational modeling · Pennes bioheat equation

1 Introduction

Chronic pain is one of the most common problems of advancing age. Although, conservative management (physical therapy and analgesics such as nonsteroidal anti-inflammatory drugs) is effective in chronic pain treatments, it only confers short-term benefits, as it is expensive, and may have significant adverse effects. The primary goal

I. Rojas et al. (Eds.): IWBBIO 2019, LNBI 11466, pp. 418–429, 2019.
https://doi.org/10.1007/978-3-030-17935-9_38

of the physicians responsible for the management of chronic pain is to target long-term solutions rather than short-lived interventions [1]. Nonsurgical minimally invasive options for treating the chronic pain have also surged during the past decades that are focused on targeting nerves transmitting pain signals. Importantly, for ablation of nervous system elements during chronic pain management, there are several main nonsurgical treatment modalities, viz., cryoablation (use of extreme cold), various laser therapies, including recent "point-and-shoot" techniques, high temperature radiofrequency, and chemical neurolysis, such as alcohol or phenol. Among the available nonsurgical modalities to alleviate chronic pain, radiofrequency ablation (RFA) offers the advantage of being precise, reproducible, cheap and effective to a great extent [1].

The application of RFA is well pronounced for treating various tumors in liver, lung, kidney, bones, prostate, and breast [2]. However, with regard to the chronic pain management, the first study of RFA application was reported in 1960s [3] and subsequently several noticeable studies have been reported for the treatment of chronic low back pain [4], chronic hip pain [5], chronic knee pain [6], and chronic head ache [7]. Importantly, during RFA, a high frequency alternating current in the frequency range of 500 kHz is applied in the vicinity of a nerve via an electrode, leading to neurodestructive thermocoagulation, thereby degrading its ability to conduct pain signals. The lesion produced due to the resistive heating during the RFA procedure may give pain relief for 12–18 months or longer, with minimal side effects and associated complications [8]. Further, since the largest area of thermal lesion is produced along the axis of electrode during continuous RFA, the radiofrequency electrode is precisely placed parallel to the target nerve so as to maximize the damage to the adjacent nerve fibers. Several patient specific clinical studies of RFA modality in treating chronic pain of bones have already been performed and reported in the literature, though questions regarding anatomical targets, selection criteria, and evidence for effectiveness, are still prevalent [9].

Numerical modeling and simulations provide a powerful tool to predict such important characteristics as the temperature distribution and lesion volume during RFA. They give a quick, convenient and inexpensive *a priori* information during the treatment planning stage of the modality to the medical practitioners. The present study is one of the initial efforts, focusing on the mathematical modeling of RFA in treating chronic pain within the bones. The main motivation and important novelty of this study is to quantify the effect of target nerve distance from the bone on the efficacy of the continuous RFA procedure.

2 Mathematical Modeling of the RFA Procedure

A three-dimensional simplified model comprising of muscle, bone and nerve tissue has been considered in the present numerical study as depicted in Fig. 1. The RFA procedures have been performed utilizing a 22-gauge needle monopolar electrode inserted parallel to the periphery of target nerve. The active tip length of the RF electrode has been considered to be 5 mm [10]. In what follows, the effect of spacing between the target nerve and the bone tissue on the efficacy of the continuous RFA will be quantified. Importantly, these studies have been performed for different values of spacing

between the nerve and the bone, viz., 0 mm (no spacing), 3 mm and 5 mm. The material properties considered in the present study are given in Table 1 [11–13]. The initial voltage and initial temperature of the entire computational domain have been considered to be 0 V and 37 °C, respectively. A constant voltage source has been applied at the active tip length of the RF electrode. The dispersive ground electrode has been modelled by utilizing a zero voltage electric potential on the outer boundaries of the analyzed domain. At each interface of our computational domain, electrical and thermal continuity boundary conditions have been imposed.

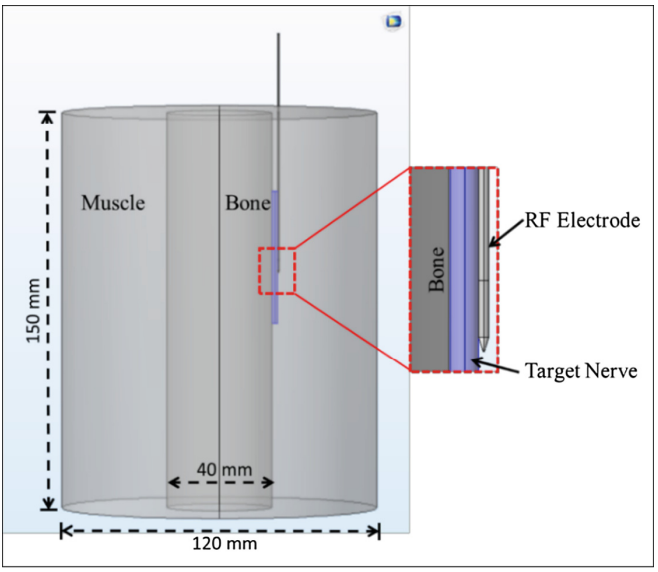

Fig. 1. Three-dimensional heterogeneous computational domain comprising of muscle, bone, nerve and RF electrode. (Color figure online)

Table 1. Electric and thermo-physical properties of different materials applied in this study (500 kHz) [11–13].

Material (Tissue/Electrode)	Electrical conductivity σ [S/m]	Specific heat capacity c [J/(kg · K)]	Thermal conductivity k [W/(m · K)]	Density ρ [kg/m^3]	Blood perfusion ω_b [s^{-1}]
Muscle	0.446	3421	0.49	1090	6.35×10^{-4}
Bone	0.0222	1313	0.32	1908	4.67×10^{-4}
Nerve	0.111	3613	0.49	1075	3.38×10^{-3}
Plastic	10^{-5}	1045	0.026	70	–
Electrode	7.4×10^{6}	480	15	8000	–
Blood	–	3617	–	1050	–

A simplified version of Maxwell's equations, known as quasi-static approximation, has been used to compute the electric field distribution within the computational domain. It is given by

$$\nabla \cdot (\sigma(T)\nabla V) = 0, \tag{1}$$

where σ is the temperature-dependent electrical conductivity (S/m) and V is the electric potential (V), which is related to the electric field "E" (V/m) by the standard potential field relationship:

$$\mathrm{E} = -\nabla V. \tag{2}$$

Further, the current density "J" (A/m^2) can be obtained from the electrical conductivity and field as follows:

$$\mathrm{J} = \sigma \mathrm{E}. \tag{3}$$

The volumetric heat generation rate Q_p (W/m^3) due to RFA is evaluated by

$$Q_p = \mathrm{J} \cdot \mathrm{E}. \tag{4}$$

The heat transfer phenomenon during RFA of target nerve has been analyzed based on the application of Pennes bioheat equation

$$\rho c \frac{\partial T}{\partial t} = \nabla \cdot (k \nabla T) - \rho_b c_b \omega_b (T - T_b) + Q_m + Q_p, \tag{5}$$

where ρ is the density (kg/m^3), c is the specific heat (J/(kg · K)), k is the thermal conductivity (W/(m · K)), ρ_b is the density of blood (1050 kg/m^3), c_b is the specific heat capacity of blood (3617 J/(kg · K)), ω_b is the blood perfusion rate (1/s), Q_p is the heat source generated by RF power (W/m^3) and is computed by using Eq. 4 above, Q_m is the metabolic heat generation (W/m^3) that has been neglected in present study, see, e.g., [12] for relevant motivations, T_b is the blood temperature (37 °C), T is the tissue temperature computed from Eq. 5 and t is the time (s).

We note that the model for the heat transfer used here allows several straightforward generalizations. Firstly, a fully coupled thermoelastic model, accounting for possible nonlinear effects, would be a natural way to improve on the present consideration of the Pennes bioheat equation. Such models, along with efficient numerical procedures for their implementations, were developed before in the context ultrashort-pulsed lasers (e.g., [13–15]), with an increasing range of medical applications currently in place. A number of them are connected with nanosecond pulsed laser heating techniques [16], as well as with thermoplasmonics applications in medicine [17], where the goal is to create highly specific therapies by inactivating dysfunctional protein molecules (the field known as molecular hyperthermia). Another avenue for an extension of the current model is to account for the finite speed of heat propagation through thermal relaxation models (e.g., [18, 19]). Such extensions have not been developed in the context of RFA procedures and they warrant a separate investigation.

In the present computational study, the tissue blood perfusion rate has been modelled using a piecewise model [20], whereby the blood perfusion rate remains at a constant predefined value below the tissue temperature of 50 °C and beyond that temperature it ceases due to the collapse of microvasculature, and is given by

$$\omega_b(T) = \left\{ \begin{matrix} \omega_{b,0} & \text{for } T < 50\,^{\circ}\text{C} \\ 0 & \text{for } T \geq 50\,^{\circ}\text{C} \end{matrix} \right\}, \tag{6}$$

where $\omega_{b,0}$ is the constant blood perfusion rate of the different tissues given in Table 1 and T is the unknown temperature computed from Eq. 5.

It is noteworthy to mention that, the lethal temperature range during RFA of nerve ablation is considered to be at or above 45–50 °C [10]. Henceforth, in the present numerical study, the ablation volume (V) has been quantified by the isotherm of 50 °C (i.e. the volume within the computational domain having temperature ≥ 50 °C for the post-RFA procedure). It is given by [21]

$$\dot{V} = \iiint_{\Omega} dV(\text{mm}^3) \quad (\text{where } \Omega \geq 50\ ^{\circ}\text{C}). \tag{7}$$

A finite element method based on the COMSOL Multiphysics 5.2 software [22] has been used to solve the coupled thermo-electric problem of the nerve ablation for treating chronic pain of bones. The computational domain has been discretized using a heterogeneous tetrahedral mesh elements using COMSOL's built-in mesh generator. A further refinement closer to the active tip of the electrode has been applied so as to accurately capture the electrical and thermal gradients. A convergence analysis has been carried out with the mesh refinement study. The final mesh comprises of 174486 elements and 476384 degrees of freedom. Further, the tissue thermal conductivity (k) has been modeled as constant [12], while the tissue electrical conductivity has been modeled by a linearly increasing (+2% per °C) function of temperature [2]. The coupled thermo-electric problem has been solved using the "multifrontal massively parallel sparse direct solver" (MUMPS) for estimating the electric field and the iterative conjugate gradient method for solving the temperature field. The maximum absolute tolerance has been set to be 10^{-3} for the time-dependent solver and the method used was based on the backward differentiation formula (BDF).

3 Results and Discussion

During the RFA procedure, ionic agitation is induced as the high-frequency alternate current interacts with the biological tissue, which is transformed into heat and propagate into the more peripheral areas by virtue of thermal conduction. The generated ionic (frictional) heating within the biological tissue leads to thermal coagulation within a few seconds above the temperature of 50 °C. Moreover, the temperatures beyond 100 °C during the RFA procedure would result in tissue boiling, vaporization and charring that usually leads to a drastic decline in electrical and thermal conductivities of the biological tissues [23, 24]. The charring phenomenon results in the abrupt rise in the electrical

impedance of the tissue, thereby limiting any further conduction of the thermal energy to more peripheral areas from the RF electrode [2]. Thus, the charred tissue around the RF electrode acts as a barrier that limits the energy deposition and reduces the lesion size generated during the RFA procedure. To address this charring problem of RFA, in our computational study we carry out a sensitivity analysis to estimate the applied voltage at the active length of the RF electrode. The goal of this sensitivity analysis has been to find an appropriate value of the applied voltage whereby the maximum temperature does not exceeds 100 °C (i.e. leading to charring), at least till the first 50 s of the RFA procedure. The applied voltage values during the sensitivity study have been varied from 10 to 25 V, that basically lies within the limit of United States Food and Drug Administration (FDA) approved commercial RFA devices available in the market and reported in the previous clinical studies [25]. The time at which charring temperatures occurred has been found to be 50 s, 10 s and 4 s for the applied voltages of 15 V, 20 V and 25 V, respectively. Further, for the applied voltage of 10 V, although no charring has taken place till the 3 min duration of RFA, the maximum temperature for this voltage was limited to only 72.67 °C. Based on the conducted sensitivity study, applied voltage of 15 V has been found to be the most appropriate level of applied energy for the computational study that can restrict the occurrence of charring at least close to the first minute of the RFA procedure.

As mentioned earlier, one of our main motivations for the present numerical study is to evaluate the effect of target nerve location from the considered bone on the efficacy of the RFA procedure. Primarily, three locations have been selected, viz., (a) no gap between the target nerve and the bone (0 mm gap), (b) 3 mm distance between the target nerve and the bone, and (c) 5 mm distance between the target nerve and the bone. The choice of selection of such distances between the target nerve and the bone during the RFA application for chronic pain relief has been motivated by [26]. Figure 2 depicts the variation of the temperature at the tip of RF electrode with ablation time for the three cases mentioned above. As evident from Fig. 2, the temperature profile is on the lower side when there is no gap between the nerve and the bone. For the cases based on 3 mm and 5 mm distances between the target nerve and the bone, the time at which charring occurred has been found to be 35 s and 31 s, respectively, as compared to the 50 s for the case of 0 mm gap.

Further, the propagation of the damage to the target nerve (corresponding to the isotherm of 50 °C) with treatment time has been presented in Fig. 3. As follows from the analysis of this figure, the ablation volume after 30 s of the RFA procedure is on a lower side for the case having no gap between the target nerve and the bone. This can be attributed to the fact that the bones have lower thermal and electrical conductivities as compared to those of nerve and muscle (*see* Table 1). The lower electrical and thermal conductivities of the bones in the heterogeneous computational model do not allow an efficient conduction of the heat on one side of the electrode. This would results in either, more requirements on the input energy with the same treatment time or in an increase in the treatment time with the same input energy, for attaining an identical volume of nerve ablation. Thus, the distance between the bone and the target nerves significantly effects the efficacy of the RFA procedure during nerve ablation, by either resulting in the increment of the treatment time or requirements of more energy input.

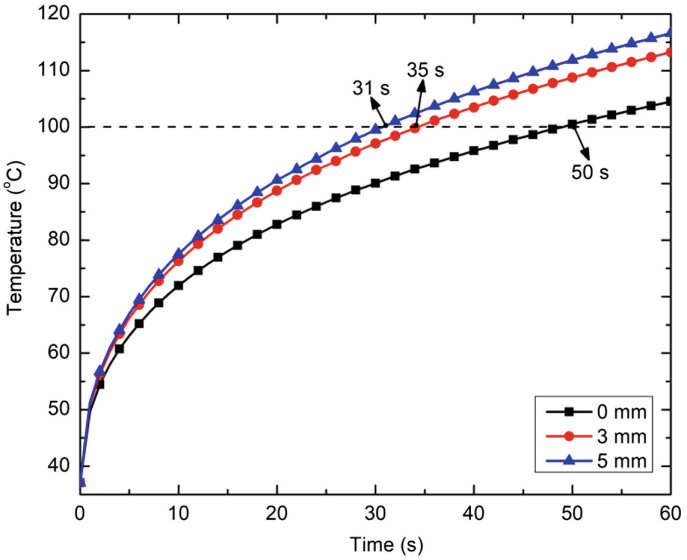

Fig. 2. Temperature distribution as a function of time monitored at the tip of the RF electrode for three different cases, viz., 0 mm, 3 mm and 5 mm distance between the target nerve and the bone. (Color figure online)

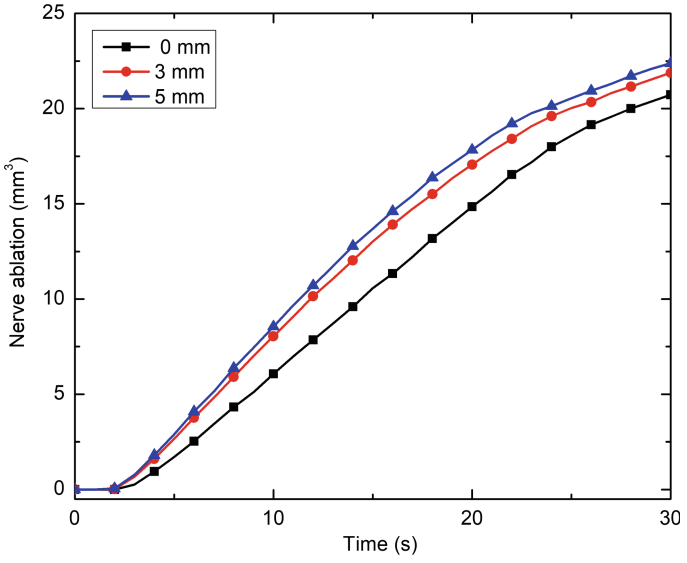

Fig. 3. Variation of nerve damage as a function of treatment time for different cases considered in the present study. (Color figure online)

Figure 4 presents the temperature distribution at a point that lies within the centre of the nerve and along a perpendicular direction from the tip of the RF electrode. As evident from Fig. 4, the time required for attaining the lethal temperature of 50 °C at the centre of the target nerve during the RFA procedure varies significantly. The time required for attaining the lethal temperature at the centre of nerve slightly decreases as the distance between the target nerve and the bone increases during the RFA procedure.

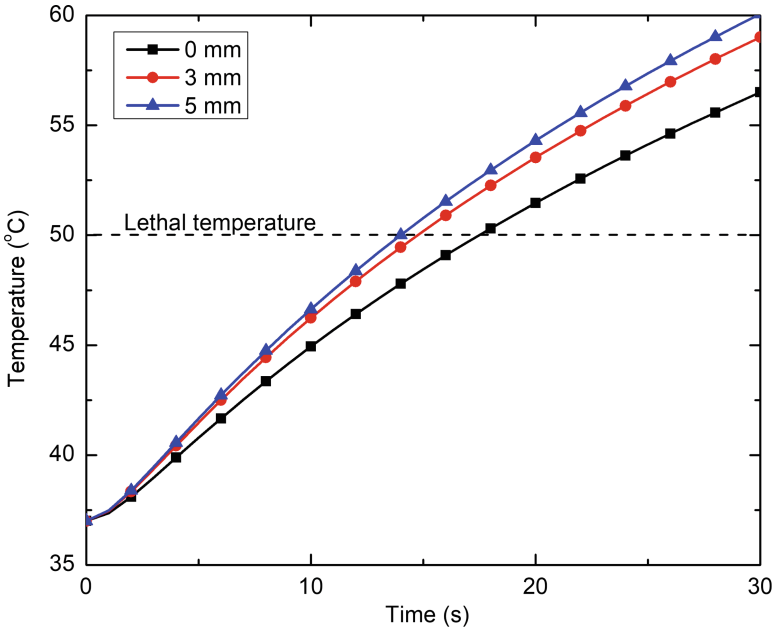

Fig. 4. Temperature distribution as a function of time monitored at the centre of nerve along perpendicular axis from the tip of the RF electrode for different cases considered in the present study. (Color figure online)

Figure 5 shows the variation of temperature along a line drawn perpendicular to the electrode axis from the tip of the RF electrode after 30 s of the RFA procedure. It can be seen from Fig. 5 that there prevails an asymmetry in the temperature profile from the electrode axis on the nerve side. Further, the asymmetric variation is more pronounced for the cases where the nerve is positioned closer to the bone tissues. This asymmetric nature could be partly attributed to the lower electrical and thermal conductivities of the bone surrounding the nerve tissue and partly due to the higher blood perfusion rate of the nerve in comparison to the muscle tissue, as seen from the analysis of Table 1. The consequence of this heterogeneous variation in the electrical and thermo-physical properties of considered tissues is that the ionic (frictional) heat generated during RFA would be easily propagated to the muscle side as compared to the nerve side. Thus, one

of the severe drawbacks of such a technique could be excessive damage to the muscle tissue or some critical structures surrounding this area. This justifies an increasing demand in patient-specific modelling and simulations for performing safe and reliable RFA of the target nerve by optimising the thermal dosage. It is expected that future studies will be addressing this issue by developing more realistic patient-specific models in collaboration with hospitals and clinicians.

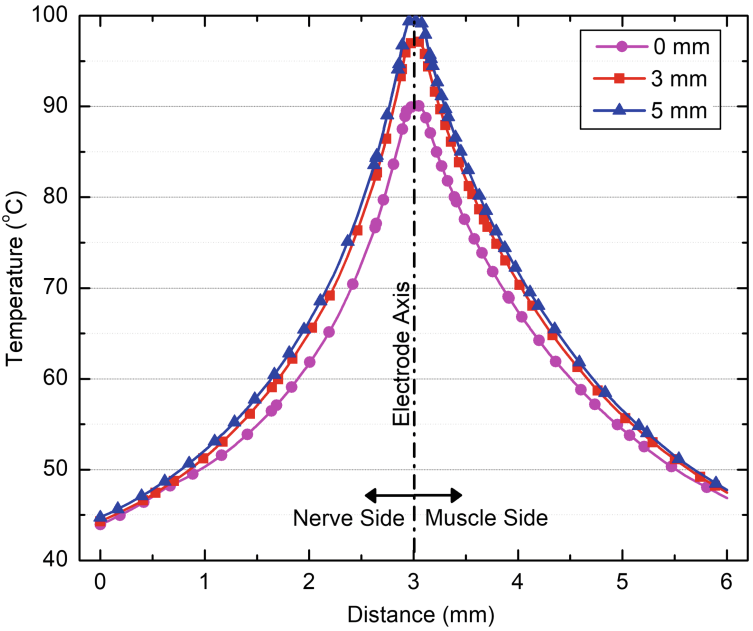

Fig. 5. Temperature distribution obtained after 30 s of the RFA procedure as a function of distance from the RF electrode axis (measured perpendicular to electrode tip). (Color figure online)

Finally, we note that Fig. 6 represents the propagation of the lesion volume attained with different time steps during the RFA procedure for the case having no gap between the target nerve and the bone. Again, the asymmetric variation can be clearly seen from the analysis of this figure, which is more pronounced for lower time steps and diminishes with the passage of time. One of the limitations of the present computational study is the lack of experimental validation of the proposed model. However, to the best of authors' knowledge, no experimental data is available in the literature for addressing this issue, specifically while considering heterogeneous surroundings. Although several experimental studies previously reported in the literature are pertinent to the present study, they have been performed utilizing only homogeneous agar-based phantom [12], egg white phantom [27], and ex-vivo liver [10].

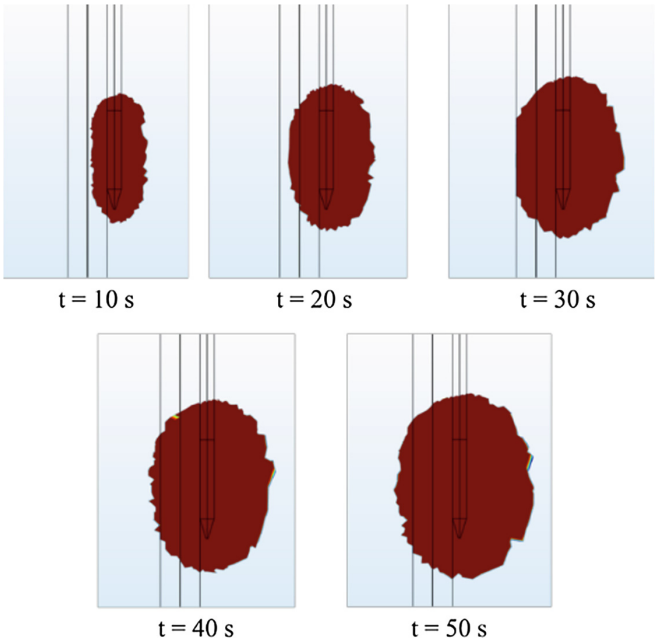

Fig. 6. Propagation of the lesion volume (corresponding to the 50 °C isotherm) obtained for different time steps during the RFA procedure. (Color figure online)

4 Conclusion

In this work, a numerical study has been carried out to evaluate appropriate values of the applied voltage suitable for performing the continuous RFA of the target nerve mitigating the occurrence of charring, an undesirable phenomenon, observed at temperatures greater than 100 °C. Further, the effect of the distance between the target nerve and the analyzed bone has been evaluated in the context of the efficacy of the continuous RFA. Based on the results obtained from this study, it has been found that there prevails a strong dependence of the distance between the target nerve and the bone on the outcomes of the RFA. The nerve ablation volume decreases for the target nerve located closer to the bone and vice versa. It is expected that the results presented in this study would assist the researchers to better recognize the variation in the outcomes of RFA associated with the target nerve location. Subsequently, as our study demonstrates, it is critical to focus on evaluating the effect of heterogeneous surrounding in the analysis of nerve ablation for treating chronic pains, rather than focusing only on oversimplified studies based on the homogeneous surrounding assumption. We also expect that future studies in this field will increasingly connect to patient-specific data, assisting the clinicians in better optimizing the thermal dosages for enabling safe and reliable RFA applications in pain mitigation.

Acknowledgements. Authors are grateful to the NSERC and the CRC Program for their support. RM is also acknowledging support of the BERC 2018–2021 program and Spanish Ministry of Science, Innovation and Universities through the Agencia Estatal de Investigacion (AEI) BCAM Severo Ochoa excellence accreditation SEV-2017-0718.

References

1. Soloman, M., Mekhail, M.N., Mekhail, N.: Radiofrequency treatment in chronic pain. Expert Rev. Neurother. **10**(3), 469–474 (2010)
2. Singh, S., Repaka, R.: Temperature-controlled radiofrequency ablation of different tissues using two-compartment models. Int. J. Hyperthermia. **33**(2), 122–134 (2017)
3. Sweet, W.H., Mark, V.H., Hamlin, H.: Radiofrequency lesions in the central nervous system of man and cat: including case reports of eight bulbar pain-tract interruptions. J. Neurosurg. **17**, 213–225 (1960)
4. Leggett, L.E., et al.: Radiofrequency ablation for chronic low back pain: a systematic review of randomized controlled trials. Pain Res. Manage. **19**(5), 146–154 (2014)
5. Bhatia, A., Yasmine, H., Philip, P., Steven, P.C.: Radiofrequency procedures to relieve chronic hip pain: an evidence-based narrative review. Reg. Anesth. Pain Med. **43**(1), 72–83 (2018)
6. Bhatia, A., Philip, P., Steven, P.C.: Radiofrequency procedures to relieve chronic knee pain: an evidence-based narrative review. Reg. Anesth. Pain Med. **41**(4), 501–510 (2016)
7. Abd-Elsayed, A., Kreuger, L., Wheeler, S., Robillard, J., Seeger, S., Dulli, D.: Radiofrequency ablation of pericranial nerves for treating headache conditions: a promising option for patients. Ochsner J. **18**(1), 59–62 (2018)
8. Collighan, N., Richardson, J.: Radiofrequency lesioning techniques in the management of chronic pain. Anaesth. Intensive Care Med. **9**(2), 61–64 (2008)
9. Jamison, D.E., Cohen, S.P.: Radiofrequency techniques to treat chronic knee pain: a comprehensive review of anatomy, effectiveness, treatment parameters, and patient selection. J. Pain Res. **11**, 1879 (2018)
10. Cosman Jr., E.R., Cosman Sr., E.R.: Electric and thermal field effects in tissue around radiofrequency electrodes. Pain Med. **6**(6), 405–424 (2005)
11. Hasgall, P.A., Gennaro, F.D., Baumgartner, C., et al.: IT'IS database for thermal and electromagnetic parameters of biological tissues. Version 4.0, 15 May 2018. https://doi.org/10.13099/vip21000-04-0.itis.swiss/database
12. Ewertowska, E., Mercadal, B., Muñoz, V., Ivorra, A., Trujillo, M., Berjano, E.: Effect of applied voltage, duration and repetition frequency of RF pulses for pain relief on temperature spikes and electrical field: a computer modelling study. Int. J. Hyperthermia. **34**(1), 112–121 (2018)
13. Zhang, S., Dai, W., Wang, H., Melnik, R.V.N.: A finite difference method for studying thermal deformation in a 3D thin film exposed to ultrashort-pulsed lasers. Int. J. Heat Mass Transf. **51**(7–8), 1979–1995 (2008)
14. Wang, H.J., Dai, W.Z., Melnik, R.V.N.: A finite difference method for studying thermal deformation in a double-layered thin film exposed to ultrashort pulsed lasers. Int. J. Therm. Sci. **45**(12), 1179–1196 (2006)
15. Wang, H., Dai, W., Nassar, R., Melnik, R.V.N.: A finite difference method for studying thermal deformation in a thin film exposed to ultrashort-pulsed lasers. Int. J. Heat Mass Transf. **49**(15–16), 2712–2723 (2006)

16. Liu, J., et al.: Behavior of human periodontal ligament cells on dentin surfaces ablated with an ultra-short pulsed laser. Scientific Reports **7**(1) (2017). Article number 12738
17. Kang, P., et al.: Molecular hyperthermia: spatiotemporal protein unfolding and inactivation by nanosecond plasmonic heating. Small **13**(36), (2017). Article number 1700841
18. Melnik, R.V.N., Strunin, D.V., Roberts, A.J.: Nonlinear analysis of rubber-based polymeric materials with thermal relaxation. Numer. Heat Transf. Appl. **47**(6), 549–569 (2005)
19. Strunin, D.V., Melnik, R.V.N., Roberts, A.J.: Coupled thermomechanical waves in hyperbolic thermoeleasticity. J. Therm. Stresses **24**(2), 121–140 (2001)
20. Scott, S.J., Salgaonkar, V., Prakash, P., Burdette, E.C., Diederich, C.J.: Interstitial ultrasound ablation of vertebral and paraspinal tumours: parametric and patient-specific simulations. Int. J. Hyperthermia. **30**(4), 228–244 (2014)
21. Singh, S., Repaka, R., Al-Jumaily, A.: Sensitivity analysis of critical parameters affecting the efficacy of microwave ablation using Taguchi method. Int. J. RF Microw. Comput. Aided Eng. e2158 (2018). https://doi.org/10.1002/mmce.21581
22. COMSOL Multiphysics® v. 5.2. www.comsol.com. COMSOL AB, Stockholm
23. Makimoto, H., Metzner, A., Tilz, R.R., et al.: Higher contact force, energy setting, and impedance rise during radiofrequency ablation predicts charring: new insights from contact force-guided in vivo ablation. J. Cardiovasc. Electrophysiol. **29**(2), 227–235 (2018)
24. Zhang, B., Moser, M.A.J., Zhang, E.M., Luo, Y., Liu, C., Zhang, W.: A review of radiofrequency ablation: large target tissue necrosis and mathematical modelling. Physica Med. **32**(8), 961–971 (2016)
25. Calodney, A., Rosenthal, R., Gordon, A., Wright, R.E.: Targeted radiofrequency techniques. In: Racz, G.B., Noe, C.E. (eds.) Techniques of neurolysis, pp. 33–73. Springer, Cham (2016). https://doi.org/10.1007/978-3-319-27607-6_3
26. Franco, C.D., Buvanendran, A., Petersohn, J.D., Menzies, R.D., Menzies, L.P.: Innervation of the anterior capsule of the human knee: implications for radiofrequency ablation. Reg. Anesth. Pain Med. **40**(4), 363–368 (2015)
27. Heavner, J.E., Boswell, M.V., Racz, G.B.: A comparison of pulsed radiofrequency and continuous radiofrequency on thermocoagulation of egg white in vitro. Pain Physician **9**(2), 135–137 (2006)